RSC Advances

PAPER

View Article Online
View Journal | View Issue

Cite this: *RSC Adv.*, 2025, **15**, 14410

Development of a point-of-care-testing platform: localized surface plasmon resonance biosensor for rapid ABO/Rh blood typing†

Pengcheng Wang,‡[a] Yan Chen,‡[b] Mingdi He,‡[c] Yan Ma,[c] Jiang Zhu,[a] Yunhuang Yang[a] and Rui Hu *[a]

Received 17th March 2025
Accepted 30th April 2025

DOI: 10.1039/d5ra01921d

rsc.li/rsc-advances

Point-of-care testing (POCT) devices are crucial for clinical diagnosis. Presently, clinical biochemical testing heavily relies on advanced analytical equipment, often necessitating bulky machinery and extended assay periods. This study presents a localized surface plasmon resonance biosensor-based POCT platform that integrates microfluidic methods for rapid and cost-effective detection of ABO/Rh blood types. The autonomous system enables high-throughput detection of ABO/Rh blood types with high specificity and sensitivity within 20 minutes using a spectrum based readout. Additionally, we have integrated eight internal microfluidic channels into the portable system to facilitate a high-throughput detection solution. Moreover, the incorporation of microfluidic channels minimizes sample cross-contamination, thereby enhancing detection precision. We believe this rapid, convenient, and cost-effective blood typing platform can serve as a valuable tool in clinical POCT applications.

1. Introduction

In recent years, there has been an increased demand for sensitive, specific, and robust testing devices in clinical diagnosis, healthcare, food safety control, and environmental monitoring.[1] Currently, colorimetric, fluorescence, electrochemical, chemiluminescent, and liquid crystal-based assays have been developed for biosensing applications owing to their excellent sensitivity and high selectivity.[2–6] However, large equipment is still required, limiting their usage to laboratory conditions only. Furthermore, fluorescent dyes and quantum dots used in these methods are limited by biological toxicity and complex fabrication procedures, restricting their application in rapid clinical diagnosis of acute pancreatitis. In this context, the emergence of POCT devices with simple, light-weight, low-cost and rapid detection has facilitated the development of devices suited for out-of-the-laboratory applications without dedicated instruments and laboratory conditions for sensing, detection and analysis.[7]

Several studies[8–11] have detailed various signal read-out systems for POCT strategies, encompassing fluorescence, ELISA assay, and chemiluminescence assays. Among these technologies, Localized Surface Plasmon Resonance (LSPR) stands out as a promising avenue for POCT by converting bioreaction signals into spectral signals. Specifically, LSPR supported by noble metal nanocrystals and nanostructures can concentrate incident light into nanoscale spatial regions, enabling various crucial applications,[12] like surface-enhanced Raman scattering and biosensing. In comparison to traditional and commercially available sensors reliant on propagating Surface Plasmon Resonance (SPR), LSPR sensors offer simplicity, cost-effectiveness, and suitability for measuring local refractive index changes due to the adsorption of target biomolecules.[13,14] Furthermore, SPR devices typically necessitate large-scale, expensive equipment, intricate optics, and precise component alignment. Conversely, LSPR sensors present distinct advantages for POCT applications, featuring simpler structures, lower costs, easier miniaturization, and label-free detection. Consequently, as an alternative to conventional bulk SPR sensors, LSPR biosensors have been proposed for developing miniaturized biosensors. Thus, with advancements in miniaturized UV-Vis light spectrometers and portable computing, LSPR biosensor configurations can be downsized to package-box sizes. This facilitates the streamlined design of LSPR devices tailored for POCT diagnostic applications.

Moreover, over the last decades, microfluidic devices have found widespread applications across diverse fields.[15–18] Poly(dimethylsiloxane)-based (PDMS-based) technology stands

[a]*State Key Laboratory of Magnetic Resonance Spectroscopy and Imaging, Innovation Academy for Precision Measurement Science and Technology, Chinese Academy of Sciences – Wuhan National Laboratory for Optoelectronics, Huazhong University of Science and Technology, Wuhan 430071, China. E-mail: hurui@apm.ac.cn*

[b]*Wuhan Fourth Hospital, Wuhan 430030, China*

[c]*Wuhan Blood Center, Wuhan 430030, China*

† Electronic supplementary information (ESI) available. See DOI: https://doi.org/10.1039/d5ra01921d

‡ These authors contributed equally to this work and should be considered co-first authors.

as a cornerstone in biochemical analysis among these devices, primarily manufactured through soft lithography techniques. However, traditional photolithography requires skilled personnel, expensive equipment, and intricate fabrication processes within a high-maintenance cleanroom. By contrast, laser cutter technology employs poly(methylmethacrylate) (PMMA) to fabricate microchannels on double-sided adhesive tape, integrating it with a plastic slab and a glass slide to create a microdevice. Importantly, this method bypasses the need for costly photolithography instruments. Well-designed microchannels can achieve both high-throughput detection and prevent sample cross-contamination effectively. Therefore, coupling LSPR biosensors with microfluidic devices significantly enhances the detection capabilities of POCT devices.

Blood transfusion is widely applied in various clinical treatments for patients experiencing massive blood loss, severe anemia, and coagulation defects. Each year, it's estimated that more than 75 million units of blood are collected and transfused to address various clinical issues, particularly critical lifesaving procedures.[19–21] Consequently, matching the donor's blood group with the patient's is crucial because agglutination resulting from incorrect blood group transfusions can lead to fatal consequences. The International Society of Blood Transfusion (ISBT) classifies blood groups into several systems. Among these groups, ABO and RhD are two of the most clinically significant major blood types, distinguished by the presence or absence of isoagglutinins A, B, and/or D on the surface of red blood cells (RBCs).[22] However, due to the lack of a robust, reliable bedside pretransfusion test method, several cases of ABO incompatible transfusions are still reported worldwide every year. Hence, there is still a need for a reliable and highly sensitive POCT method for blood transfusions.

This study introduces an LSPR-based POCT platform designed for clinical diagnostic applications. To minimize required equipment, we opted for a portable spectrometer as optical sensors for detecting LSPR spectra. Simultaneously, we utilized bio-functionalized gold nanoparticles (NPs) in LSPR biochips for specific binding of target biomolecules. This greatly simplifies and enhances the flexibility of optical alignment and light coupling compared to a prism-based SPR configuration. The LSPR-based POCT platform doesn't necessitate large or expensive optical components. Optical components and sensing elements are interconnected using optical fibers and affixed onto the portable spectrometer. Additionally, eight microfluidic channels were integrated into the current POCT platform to enable high-throughput testing. To determine the optimal biosensing capability (plasmonic sensitivity) of the POCT platform, a proof-of-concept LSPR sensing of RBCs was conducted. This study presents an LSPR-based POCT platform as a rapid and robust method for ABO/Rh blood typing.

2. Materials and methods

2.1 Materials

11-Mercaptoundecanoic acid, *N*-(3-dimethylaminopropyl)-*N*′-ethylcarbodiimide hydrochloride, *N*-hydroxysuccinimide, and bovine serum albumin were purchased from Sigma-Aldrich (Schnelldorf, Germany). Ethanol, acetone, chloroform, and carbon tetrachloride were acquired from Sigma-Aldrich (Schnelldorf, Germany). Phosphate-buffer saline (PBS buffer, pH 7.4), carbonate buffer solution (CBS buffer, pH 9.6), and acetate buffer (pH 3.6) were received from Sigma (Schnelldorf, Germany). Antibodies were provided by the Wuhan Blood Center, Wuhan, China, including anti-A mono-clonal IgM antibody (Lot: 57 014), anti-B monoclonal IgM antibody (Lot: 57 033), and anti-D (Rh) monoclonal IgG/IgM mixed antibodies (Lot: 57 011). A total of 22 RBCs samples in ethylenediaminetetraacetic acid (EDTA) blood collecting tubes were provided by Wuhan Blood Center, Wuhan. Blood grouping was identified by the Wuhan Blood Center using micro-column (gel) and the slide agglutination assay. All procedures have been approved by Wuhan Blood Center Ethics Committee and performed in accordance with the ethical standards (no. KY2024-101).

For the all the rinsing steps and dilutions, ultrapure distilled water (18.2 MΩ cm) was used, which was produced by a millipore Milli-Q water purification system (Molsheim, France). An ultrasonic water bath (Elmasonic S30H) was used for sample cleaning.

2.2 Design, fabrication of the microfluidic layer

The microfluidic layers were manufactured by using a CO_2 laser cutter (Laser Technology, Shenzhen, China), with a resolution of −100 μm. The microfluidic layer has a dimension of 25 mm × 75 mm. The microfluidic layer was fabricated by PMMA (YongChip, Zhejiang, China). Inlets and outlets were drilled on the plastic cover layer. After nitrogen-blowing-based cleaning, double-sided adhesive films were used to assemble the two layers.

2.3 Fabrication of well-organized gold NPs on glass substrate

The fabrication of gold nanoparticles (NPs) followed the procedure outlined in previous studies.[23,24] Initially, glass slides (25 mm × 75 mm) were employed as substrates for depositing a thin gold film. Prior to evaporation, the glass slides were affixed to plastic vertical sample holders and immersed in a cleaning solution comprising a mixture of detergent (Decon 90) and deionized water (in a 2 : 8, v/v ratio). Subsequently, the samples were subjected to ultrasonication in a water bath at 50 °C for 15 minutes. Following this, the cleaned samples were thoroughly rinsed with deionized water, dried under a stream of N_2, and subjected to three additional rounds of ultrasonication washing in deionized water at 50 °C for 5 min each. Next, a microfluidic layer was integrated onto the clean glass slides to serve as a mask during the gold evaporation process. For the evaporation step, the prepared glass slides with microfluidic layer masks were positioned on a circular evaporation plate with a diameter of 200 mm. Gold evaporation was carried out in an evaporator using the electron beam evaporation mode at room temperature under high vacuum conditions (pressure of 1.0×10^{-6} torr). The evaporation rate was maintained at approximately 0.01 nm s^{-1}. The thickness of the gold film was monitored using a built-in quartz crystal sensor. After evaporation,

a 4 nm gold film was coated onto the sample surface. Subsequently, the microfluidic layer masks were carefully removed from each sample, and the patterned glass slide substrates were transferred to a high-temperature oven for thermal annealing at 550 °C for 8 h in an oxygen atmosphere. This process resulted in the formation of well-organized gold nanoparticles on the glass substrate.

2.4 Surface characterization

Gold NPs were characterized by a scanning electron microscope (SEM) (S-4800, Tokyo, Japan) and an atomic force microscope (AFM) (Bruker ICON, USA) with cantilever ScanAsyst-Air in silicon nitride with a tip height of 2.5–8.0 mm. A spring constant of 4 N m^{-1} and a reflective aluminum coating on the back side in standard ScanAsyst-Air mode were used to characterized the surface of the annealed coverslips for surface morphology information.

Utilizing the microfluidic layer mask on the glass slide surface facilitated the creation of 24 well-defined, independent zones coated with gold NPs after the annealing process. For the surface characterization (SEM and AFM), three small round patterns within a single independent channel were specifically chosen in this study.

2.5 LSPR spectra measurement by optical spectrophotometer

It should be noted that the LSPR extinction spectra were measured by a home-built transmission UV-Vis optical setup including a $\emptyset = 50$ μm fiber (Oceanhood, China) coupled with an optical spectrophotometer (Oceanhood, XSM11639, China) and a white exciting light source (DL2000-ADJ, Oceahood, China). In the present study, for the annealed sample, we chose 8 independent patterns for testing LSPR spectra.

2.6 Gold NPs biofunctionalization for ABO/Rh blood typing

The annealed glass samples were first washed with an ethanol/acetone mixture solvent (1 : 1 volume ratio) in an ultrasonic water bath for 20 min at room temperature, followed by washing with ethanol and drying under N_2 stream. Further, the annealed glass substrate was immersed in 1 mL of 11-mercaptoundecanoic acid (MUA) ethanolic solution (1 mM) for 12 h at room temperature, followed by washing with ethanol and drying under N_2 stream. The carboxylic group of the thiolated surface was activated with a mixture of EDC/NHS aqueous solution (0.4 mM/0.1 mM) at room temperature for 50 min. After aqueous washing and drying, 20 μL of anti-A, -B, and -D solutions antibody diluted in phosphate-buffered saline (PBS 0.1 mg mL^{-1}) was deposited onto the metal patterns for 5 h at 4 °C. Finally, 50 μL of 1% BSA was dripped onto gold NPs for 40 min to block unbound gold NPs surface and avoid nonspecific absorption. After washing with PBS buffer and rinsing with dd-H_2O, the antibody-modified substrate was used as a biochip for blood group typing. The plasmonic spectra corresponding to each biofunctionalization step were recorded by using extinction measurements.

2.7 Biosensors platform repeatability and long-term stability

Following the completion of the biofunctionalization process, the sensor surface was thoroughly washed with phosphate-buffered saline (PBS) and rinsed with deionized water (dd-H_2O). Subsequently, blood samples (AB/Rh^+) were introduced for blood group typing. Notably, after each analytical cycle, the biosensor surface was regenerated using a 10 mM glycine solution,[25] and successive detection assays were conducted iteratively until a significant decline in sensor performance was observed, indicating the loss of functional detection capability. All the test were repeated 3 times. Moreover, to assess the long-term stability of the biosensor, biofunctionalized sensors were stored at 4 °C and subsequently employed to analyze blood samples (AB/Rh^+) after 1, 3, and 7 days of storage. Meanwhile, due to time constraints, to simulate long-term storage conditions, the biosensor was placed at 37 °C for 3 days and subsequently employed to analyze blood samples (AB/Rh^+), thereby approximating the effect of storage at 4 °C for a period of six months.[26]

2.8 Statistic analyze

SEM images were applied to estimation the size distribution of metallic NPs using the Public Domain Image J software developed by the National Institutes of Health. AFM images were analyzed using Gwyddion software to calculate the roughness information and particle analyze for samples. Origin software was used for the statistical analysis (linear regression and smooth, differentiate or integrate curve) of all the experimental data and for graphing the results.

3. Results and discussion

3.1 Working principle of the LSPR-based POCT platform

In our study, we initially investigated the capability of our LSPR-based POCT platform in distinguishing between blood types, encompassing ABO and $Rh^{\pm}$. As depicted in Fig. 1, the LSPR-based POCT platform was structured with a glass support plate, a layer of bio-functional gold NPs, a microfluidic layer, and a plastic film cover. The glass support plate served to secure the gold NPs and provided transparence for incident light to stimulate the gold NPS, thereby exciting the LSPR. The second layer comprised gold NPs, and notably, the POCT platform includes eight microfluidic channels, each housing three round testing holes (4 mm diameter). These testing holes were embedded with gold NPs and modified with anti-A, -B, and -D, respectively, for targeting specific RBCs. On top of the gold NPs layer, the microfluidic device was utilized to create eight pallet channels to facilitate high-throughput testing. This microfluidic layer consists of a PMMA layer fabricated using a CO_2 laser cutter based on a digital design. This fabrication method was rapid, cost-effective, and conducive to high-throughput production. Additionally, a plastic film cover was positioned atop the device. Using a disposable syringe connected to the inlet of the plastic film, we can apply uniform and stable positive pressure through simple hand-powered actuation. This positive pressure propels the sample flow from the syringe into

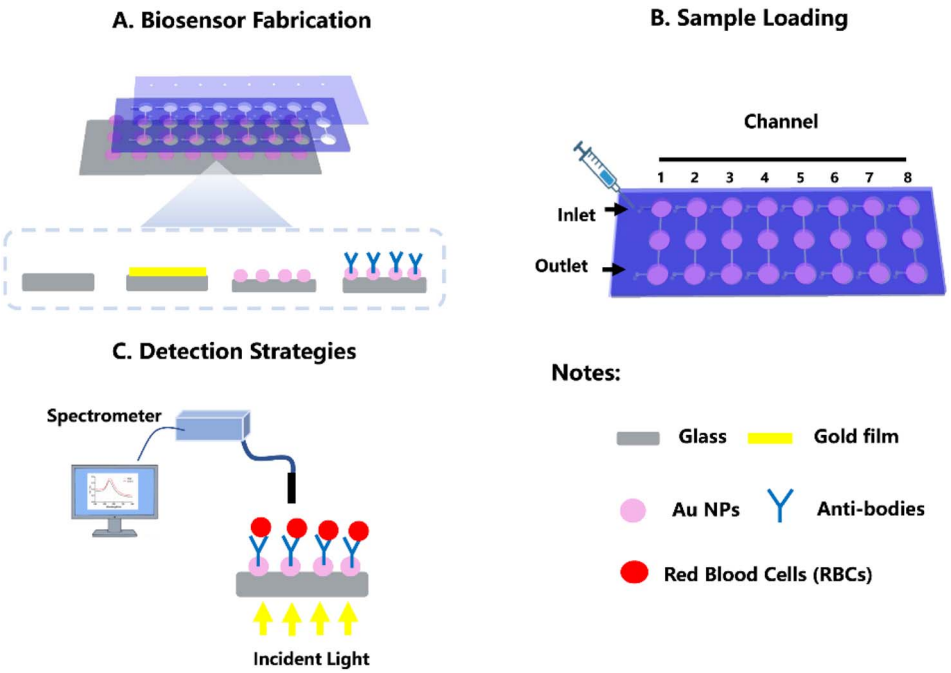

Fig. 1 Scheme of the LSPR-based POCT platform. (A) A cartoon drawing of the LSPR-based microfluidics bio-sensing system. (B) Scheme showing the sample loading method. (C) Scheme showing a brief on-chip detection protocol.

the three pretreated antibodies gold NPs reaction area. The detection mechanism hinges on the blood antigen–antibody specific reaction that occurs when RBCs interact with their corresponding antibody-treated gold NPs, leading to the binding of RBCs with gold NPs. Anti-A and anti-B antibodies recognize antigens A and B on the RBC surfaces, determining A, B, and O blood types. Meanwhile, the Rh-positive (Rh^+) antigen interacts with anti-D antibody, facilitating Rh group screening. Bound RBCs remain on the gold NPs surface, while non-binding RBCs continue flowing through the channel. This interaction enables the recognition of target RBCs by specific antibodies modified on the nanoparticle surface. The resulting biochemical interaction elevates the refractive index of the local medium, transduced by plasmonic tuning of the resonant peak, involving resonant wavelength shifts and/or maximum optical density changes, detectable by the spectrometer. Typically, the on-chip assay comprises two main steps. Initially, the blood sample is introduced into the microfluidic channel and incubated with bio-functional gold NPs for 10 min. Subsequently, after washing testing channels with dd-H_2O, the incident light irradiates the sensing areas, and the spectrometer detects the optical signal to read the testing results.

3.2 Characterization of the LSPR-based POCT platform

The fabrication process and experimental procedures for the LSPR-based POCT platform are illustrated in Fig. 1 and S6.† Specifically, the gold NPs on the solid glass substrate were produced by vacuum-evaporating a gold thin film onto a flat substrate and subsequently annealing it at high temperatures. This method was chosen for its simplicity and cost-effectiveness in generating stable and uniform gold plasmonic nanostructures on the glass substrate. Notably, the well-designed microfluidic PMMA layer on the glass substrate facilitates the creation of eight precisely defined microfluidic channels coated with a gold thin film (4 nm) following the evaporation process. These coated channels are then transformed into gold nanoparticles through thermal annealing.

To verify the well-organized gold structures and their effective LSPR properties, we performed SEM, AFM and spectrometer optical (LSPR) characterizations on the annealed samples for channel morphology observation and LSPR property analysis. The AFM image (Fig. 2 & S1†) revealed a homogeneous distribution of individual spherical gold NPs across the smooth glass surface due to their effective dispersion during high-temperature annealing (close to the glass transition temperature). The calculated average surface roughness R_q and R_a were 4.00 ± 0.43 and 5.01 ± 0.72, respectively. Analyzing SEM images revealed that the majority of gold NPs exhibited a diameter of 3–6 nm (61.28%), confirming a uniform deposition of gold NPs on the glass substrate, divided into distinct zones due to the shadowing effect of the microfluidic PMMA layer mask. Subsequently, LSPR spectra were obtained for the as-deposited sample. For the annealed samples' plasmonic property assessment, eight independent areas from each microfluidic channel of the device were selected for testing. As depicted in Fig. S1,† the annealed sample with a nominal thickness of 4 nm exhibited well-defined plasmonic peaks. Statistical data indicated that the average plasmonic resonant wavelength was located at 535.1 ± 1.5 nm, with a maximum optical density recorded as 0.147 ± 0.01. The relative standard deviation (RSD) for resonant wavelength and maximum optical density was lower than 0.28% and 5.53%, respectively, indicating

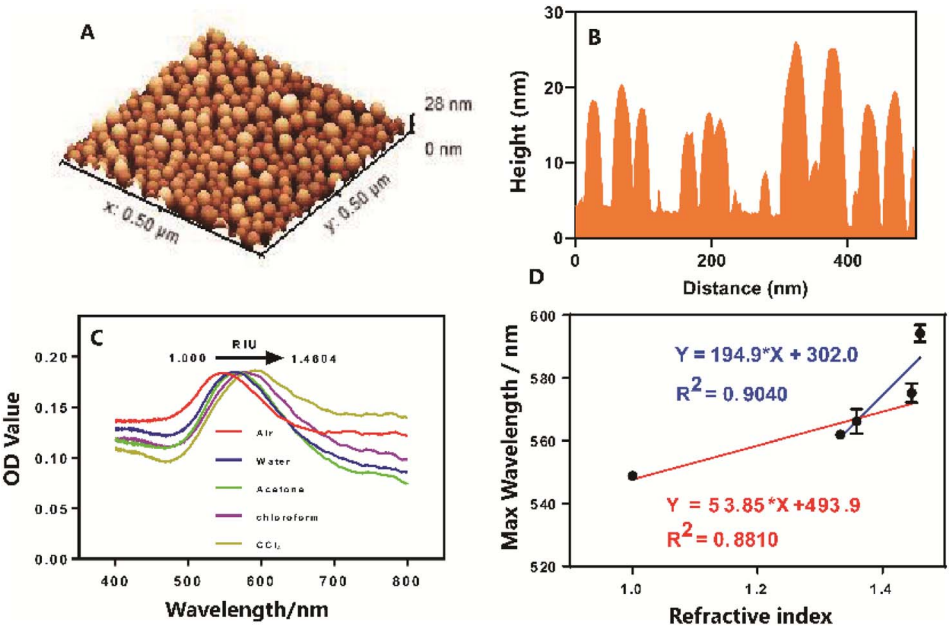

Fig. 2 (A) Microscopy (AFM) image of glass coated with gold NPs. (B) Line profile analysis of AFM image of gold NPs. (C) Sensitivity test of annealed NPs in air ($n = 1$), dd-water ($n = 1.33$), acetone ($n = 1.36$), chloroform ($n = 1.44$), and carbon tetrachloride ($n = 1.46$). (D) Linear fitting for different environments RI on gold NPs.

a homogeneous LSPR property in the obtained gold nanostructures. Moreover, as shown in the Fig. 2C and D, the plasmonic performance of the annealed samples was assessed using a home-built extinction measurement system in various surrounding environments such as air ($n = 1$), dd-water ($n = 1.33$), acetone ($n = 1.36$), chloroform ($n = 1.44$), and carbon tetrachloride ($n = 1.46$). The bulk refractive index sensitivity (S, nmper RIU) for the annealed sample was calculated based on the red shift of the resonant peak divided by changes in the refractive index (RI). As illustrated in Fig. 2, depositing 5 μL of dd-water on the annealed sample resulted in a resonant wavelength red-shift of 13.06 ± 0.70 nm. Furthermore, changes in the surrounding environment of the gold NPs with acetone, chloroform, and carbon tetrachloride induced plasmonic peak red-shifts of 6.3 ± 0.8 nm, 7.1 ± 3.1 nm, and 19 ± 3 nm, respectively. The calculated bulk refractive index sensitivity of gold NPs, particularly within the range of 550–575 nm, is provided in Table S1.† These findings underscore the remarkable sensitivity of gold NPs to variations in the surrounding refractive index.

To summarize, distinct zones of gold NPs were spatially engineered on a glass substrate, achieved through the microfluidic layer mask in conjunction with the deposition of a continuous 4 nm gold film followed by annealing at 550 °C for 8 h. Surface characterization techniques and optical measurements revealed that the annealed gold NPs exhibited a uniform size and spherical shape, displaying well-defined LSPR resonant peaks and excellent homogeneity in LSPR properties. Consequently, these findings pave the way for the potential utilization of well-organized in constructing a LSPR-based POCT platform for typing red blood cells (RBCs).

3.3 Optimize antibodies immobilization on the gold NPs

The determination of ABO/Rh blood groups hinges on the presence or absence of specific proteins and oligosaccharides (antigens) like A, B, and D, which are prominently displayed on the surface of red blood cells (RBCs). It's widely recognized that RBCs directly bind to their corresponding antibodies. To facilitate the specific detection of different RBC groups, anti-A, -B, and -D antibodies were employed for the functionalization of gold NPs. For enhanced bio-modification of gold NPs, the gold NPs' surface was activated using MUA and EDC/NHS.[27–30] Notably, a slight red-shift in the resonant wavelength was observed post MUA and EDC/NHS modification (Fig. S2†). To optimize the immobilization of anti-A, -B, and -D antibodies onto the gold NPs, various reaction buffers and a range of antibody concentrations were explored. As illustrated in Fig. 3, experimental findings indicated that the phosphate buffer (PBS) was the most conducive buffer for antibody seeding onto the gold NPs owing to its neutral pH environment. Moreover, 20 μL anti-A, -B, and -D solutions at concentrations ranging from 5 to 200 μg mL^{-1} were applied to different gold NPs. Transmission spectra of gold NPs were recorded before and after antibody immobilization. The redshift of λ_0, denoted as $\Delta\lambda = \lambda_{antibodies} - \lambda_0$, against varying concentrations of antibody proteins, was plotted in Fig. 3B–D. The $\Delta\lambda$ exhibited rapid initial growth with smaller concentrations of antibodies followed by a constant line, no concentration dependence. It is noteworthy that the shift approached a constant value when the antibodies (A, B, and D) exceeded 100 μg mL^{-1}. Therefore, in the present study, we opted for PBS buffer as the optimized reaction buffer and 100 μg mL^{-1} as the optimized concentration for antibody immobilization.

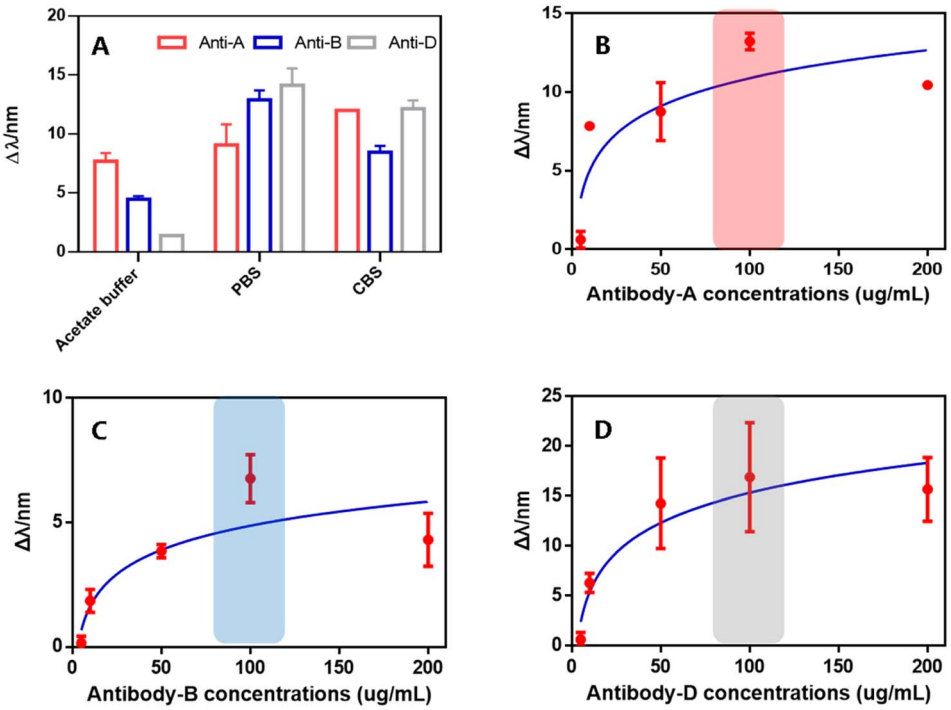

Fig. 3 (A) The plot of the shift of LSPR wavelength red-shift *versus* different buffer. (B–D) The plot of the shift of LSPR wavelength red-shift *versus* different antibodies concentration (anti-A, -B, and -D).

3.4 Specificity and sensitivity test of LSPR-based POCT platform for blood typing

This detection strategy of present biosensor is based on the high specificity of antigen–antibody interactions, where red blood cells (RBCs) react with gold nanoparticles (gold NPs) functionalized with selective antibodies. Anti-A and anti-B antibodies conjugated to the gold NP surface selectively recognize A and B antigens expressed on RBC membranes, enabling differentiation among A, B, and O blood groups. In parallel, Rh factor determination is achieved through the specific binding of Rh-positive antigens to immobilized anti-D antibodies. RBCs that express the target antigens adhere to the gold NP surface, while those lacking the corresponding epitopes remain in suspension and are carried downstream within the microfluidic channel. This molecular recognition event induces a localized increase in the refractive index, which is transduced into an optical signal *via* plasmonic resonance. Resultant spectral changes – such as shifts in resonance wavelength or alterations

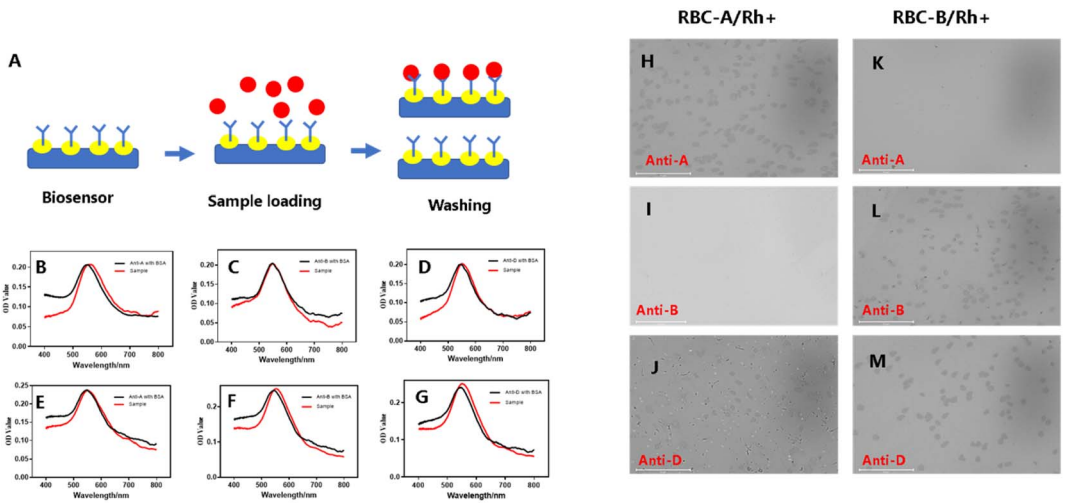

Fig. 4 LSPR-based detection for blood typing and in standard RBCs-A and -B samples. (A) Scheme showing the mechanism of the LSPR-based blood typing biosensor. (B–G) LSPR spectra of standard RBCs-A and -B samples on different antibodies binding gold NPs and their corresponding optical microscope photo (H–M).

in peak optical density – are subsequently measured using a spectrometer. It should be noted that the platform's capability to distinguish various blood types was investigated using standard A/Rh$^+$ and B/Rh$^+$ type RBCs. When blood type A/Rh$^+$ RBCs were incubated onto the anti-A/anti-D gold NPs testing area, a resonant peak red-shift of approximately 7.83 nm and 3.23 nm was observed compared to the non-incubation condition, indicative of the RBCs' attachment to the biosensor surface (Fig. 4B–D). Conversely, there was minimal change in the spectra of the anti-B gold NPs testing area after incubation with blood type A (0.46 nm red-shift). Microscopic observations revealed dense adherence of RBCs on the anti-A and anti-D gold NPs testing areas post-incubation with blood type A, while limited adherence was observed on the anti-B area, consistent with the alterations in LSPR spectra. Similar testing results were obtained with blood type B/Rh$^+$, further corroborating these findings. Consequently, the experimental results suggest that our LSPR-based POCT platform effectively captures RBCs, enabling specific identification of blood types.

Additionally, the LSPR-based POCT platform was utilized to estimate RBCs concentrations in blood samples. To establish the relationship between RBCs concentrations and LSPR resonant wavelength changes and to investigate platform sensitivity, we exposed the sensors to diluted RBCs suspensions with serial concentrations ranging from 4×10^6 to 4×10^9 cells per mL. As shown in the Fig. 5, the LSPR resonant wavelength displayed a gradual red-shift corresponding to RBCs concentrations increased. Notably, a substantial enhancement in the LSPR resonant wavelength occurred in the range of 10^7 to 10^9 cells per mL, whereas spectra differentiation was challenging at lower concentrations. Linear fitting formulas [$Y = 9.775X - 74.69$, $Y = 8.213X - 63.09$, $Y = 8.319X - 62.03$] were obtained to elucidate the relationship between different RBC concentrations and LSPR resonant wavelength shifts. In summary, these findings illustrate the exceptional detection sensitivity of the LSPR-based POCT platform for blood typing.

Moreover, to evaluate the repeatability of the biosensor, the sensing surface was regenerated using a glycine solution after each measurement. All tests were conducted using real blood samples (AB/Rh$^+$) and repeated in triplicate to ensure reproducibility. The experiment results (Fig. S6 and 7†) shown that three independent experiments demonstrated high consistency, indicating good reproducibility of the sensor performance. Meanwhile, even after second time regeneration (analytical cycle 3), the biosensor retained robust performance in blood group typing, demonstrating its reusability and repeatability. However, after third time regeneration (analytical cycle 4), a significant decline in sensor performance was observed, indicating the loss of functional detection capability. Moreover, the long-term stability test of the biosensor was conduct. The experiment results (Fig. S8†) shown that blood group detection capability of the biosensors remained consistent across various storage durations ($p > 0.05$), indicating that sensor performed excellent long-time stability.

3.5 Clinical sample testing on LSPR-based POCT platform for blood typing

To assess the practicality of our platform in analyzing patient samples, we obtained blood samples from 21 patients previously screened in clinical laboratories for blood typing. The on-chip assay procedure, as outlined in Fig. 6, was conducted on a single microfluidic channel comprising three independent anti-A, -B, and -D detection areas. Following a 10 min incubation period to facilitate RBCs binding to corresponding antibodies, the samples were subsequently analyzed using a portable spectrometer. The entire on-chip assay could be completed within 20 min, encompassing sample loading, incubation, washing, and readout time.

Fig. 6 presents the original LSPR resonant wavelength shifts observed for all clinical samples, with corresponding quantitative results and heat map results depicted in Fig. 6. A cutoff value of 2 nm was established to differentiate between negative and positive samples. Negative samples generated red-shift signals close to the negative control (<2 nm), while positive samples exhibited relatively higher red-shift values (>2 nm). The

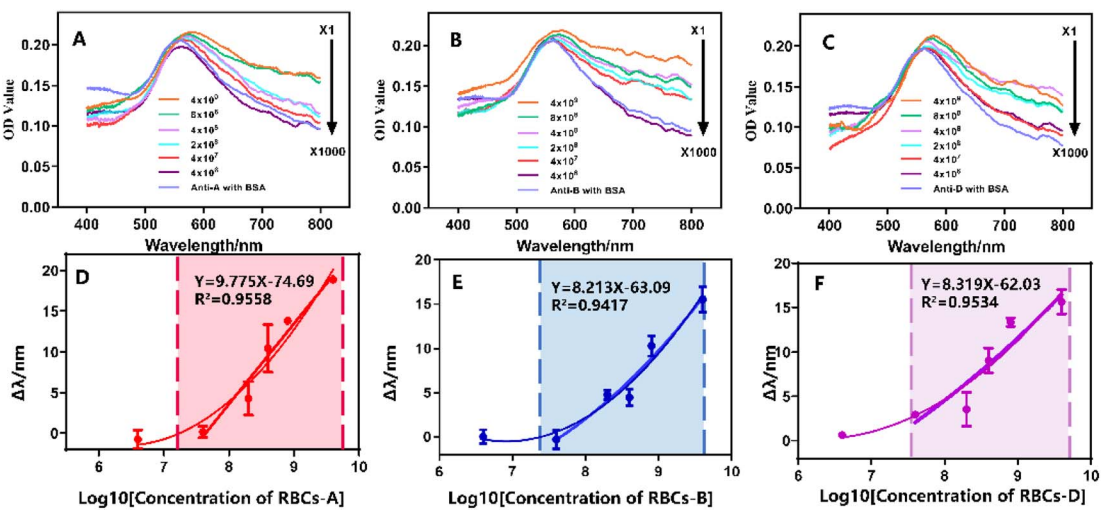

Fig. 5 LSPR spectra of different (A) RBCs-A, (B) RBCs-B, (C) RBCs-D concentrations and their corresponding calibration curves (D–E).

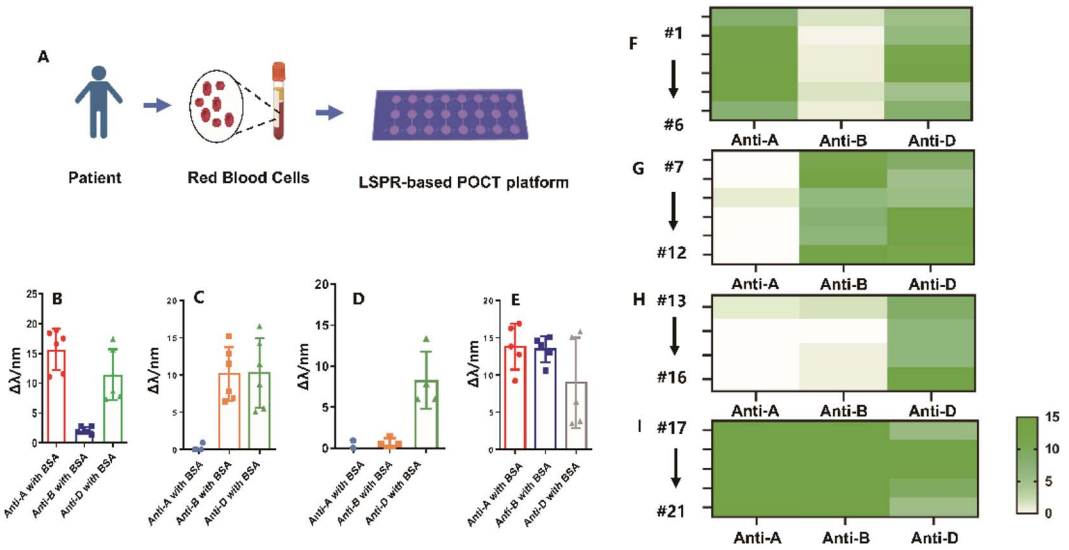

Fig. 6 Blood typing in patient samples on POCT platform. (A) Workflow of the on-chip testing based on the spectrometer readout. (B–E) LSPR red-shift showing the on-chip testing results of the 21 clinical samples. (F–I) Heatmap of the LSPR red-shift of the images in (B).

POCT platform's detection outcomes correlated well with the clinical results, notwithstanding weak positive signals for anti-B in sample #1 and #5 (2.77 and 2.76 nm red-shift, respectively). Furthermore, in cases of leukemia, a decrease in red blood cells can result in reduced surface antigens, complicating blood type identification. Conventional methods may mistakenly categorize blood samples from leukemia patients with type A blood as type O due to this antigen reduction. However, our LSPR-based POCT platform displayed sensitive detection capabilities in accurately identifying the precise blood type in these cases (Fig. S4A–D†), in contrast to conventional methods (Fig. S4E†). These outcomes highlight the reliability of the LSPR-based POCT platform for the rapid determination of blood types. Moreover, as shown in Table S2,† in the present study, we report a high-throughput localized surface plasmon resonance (LSPR) biosensor for rapid and cost-effective ABO/Rh blood type detection in point-of-care testing (POCT). This biosensor enables blood typing within 10–20 minutes using less than 1 mL of blood and does not rely on bulky instrumentation, making it well-suited for POCT applications. In comparison, a paper-based assay developed by J. Noiphung *et al.*[31] achieved a shorter detection time of approximately 10 minutes. However, it exhibited limited accuracy, with only 85% accuracy reported for type B blood typing. Additionally, the paper-based sensor is single-use and cannot be reused, limiting its practicality in high-throughput settings. The gel agglutination assay, which has been approved by the U.S. Food and Drug Administration for ABO and Rh typing,[32] demonstrates nearly 100% accuracy. Nevertheless, its operation is more complex, requiring two rounds of centrifugation lasting 5–10 minutes each. Furthermore, its dependence on bulky laboratory equipment renders it unsuitable for POCT applications and limits its scalability for high-throughput use. In contrast, our LSPR biosensor offers a more practical, cost-effective, and high-throughput solution, particularly suitable for bedside emergency testing and use in rural or resource-limited settings in developing countries.

4. Conclusions

In this work, we report a microfluidic-coupled localized surface plasmon resonance (LSPR) biosensor for rapid and cost-effective ABO/Rh blood type detection in Point-of-Care Testing (POCT). Leveraging a microfluidic layer, our platform enables convenient, high-throughput on-chip assays, ensuring swift and contamination-reduced detection directly on the microfluidic device. It achieves ABO/Rh blood typing within 20 minutes, utilizing less than 1 mL of blood sample, with a detection sensitivity of RBCs at 4×10^7 cells per mL based on spectrometer readouts. Testing clinical patient samples demonstrated a 90% consistency between the on-chip test results and those obtained through clinical tests. We believe this platform holds significant potential for POCT in clinical blood typing, especially for patients requiring emergency blood transfusions, offering promising benefits to human health.

Data availability

Data will be made available on request.

Author contributions

Conceptualization, Rui Hu, Yunhuang Yang, and Pengcheng Wang; methodology, Pengcheng Wang, Chen Yan and Mingdi He; software, Pengcheng Wang and Chen Yan; validation, Rui Hu, Yunhuang Yang and Yan Ma; formal analysis, Rui Hu, and Pengcheng Wan; investigation, Pengcheng Wang, and Mingdi He; resources, Mingdi He; data curation, Pengcheng Wang, Chen Yan, Rui Hu, and Mingdi He; writing—original draft preparation, Pengcheng Wang; writing—review and editing, Rui

Hu, Yunhuang Yang, Mingdi He, and Yan Ma; visualization, Pengcheng Wang and Jiang Zhu; supervision, Rui Hu, Yunhuang Yang; project administration, Rui Hu, Yunhuang Yang; funding acquisition, Rui Hu, Yunhuang Yang. All authors have read and agreed to the published version of the manuscript.

Conflicts of interest

The authors declare no conflict of interest or personal relationships that could have appeared to influence the work reported in this paper.

Acknowledgements

This work was supported by funds from the Strategic Priority Research Program of the Chinese Academy of Sciences (XDB0540000), the National Natural Science Foundation of China (22374155, 22327901). We thank Dr Tian Yongsheng (Wuhan University of Science and Technology) for his help in the annealing operation.

References

1 K. H. Ooi, M. M. Liu, J. W. D. Tay, S. Y. Teo, P. Kaewsapsak, S. Jin, C. K. Lee, J. Hou, S. Maurer-Stroh, W. Lin, B. Yan, G. Yan, Y. G. Gao and M. H. Tan, An engineered CRISPR-Cas12a variant and DNA-RNA hybrid guides enable robust and rapid COVID-19 testing, *Nat. Commun.*, 2021, **12**(1), 1739, DOI: 10.1038/s41467-021-21996-6.

2 E. Balaur, S. O' Toole, A. J. Spurling, G. B. Mann, B. Yeo, K. Harvey, C. Sadatnajafi, E. Hanssen, J. Orian, K. A. Nugent, B. S. Parker and B. Abbey, Colorimetric histology using plasmonically active microscope slides, *Nature*, 2021, **598**(7879), 65–71, DOI: 10.1038/s41586-021-03835-2.

3 E. Albertinale, L. Balembois, E. Billaud, V. Ranjan, D. Flanigan, T. Schenkel, D. Estève, D. Vion, P. Bertet and E. Flurin, Detecting spins by their fluorescence with a microwave photon counter, *Nature*, 2021, **600**(7889), 434–438, DOI: 10.1038/s41586-021-04076-z.

4 M. Sadasivam, A. Sakthivel, N. Narayana, *et al.*, Magnetic bead-amplified voltammetric detection for carbohydrate antigen 125 with enzyme labels using aptamer-antigen-antibody sandwiched assay, *Sens. Actuators, B*, 2020, **312**, 127985, DOI: 10.1016/j.snb.2020.127985.

5 R. W. Meek, J. N. Blaza, J. A. Busmann, M. G. Alteen, D. J. Vocadlo and G. J. Davies, Cryo-EM structure provides insights into the dimer arrangement of the O-linked β-N-acetylglucosamine transferase OGT, *Nat. Commun.*, 2021, **12**(1), 6508, DOI: 10.1038/s41467-021-26796-6.

6 C. Zhao, S. Chen, L. Zhang, D. Zhang, R. Wu, Y. Hu, F. Zeng, Y. Li, D. Wu, F. Yu, Y. Zhang, J. Zhang, L. Chen, A. Wang and H. Cheng, Miniature three-photon microscopy maximized for scattered fluorescence collection, *Nat. Methods*, 2023, **20**(4), 617–622, DOI: 10.1038/s41592-023-01777-3.

7 X. Dai, S. Wang, Y. Wang, X. Wang, X. Wu, X. Liu, J. Jiang, T. Xu and T. Liu, Dual-resonance optical fiber lossy mode resonance immunoprobe for serum PSA detection, *Biosens. Bioelectron.*, 2025, **271**, 117049, DOI: 10.1016/j.bios.2024.117049.

8 S. Chung, L. E. Breshears, A. Gonzales, C. M. Jennings, C. M. Morrison, W. Q. Betancourt, K. A. Reynolds and J. Y. Yoon, Norovirus detection in water samples at the level of single virus copies per microliter using a smartphone-based fluorescence microscope, *Nat. Protoc.*, 2021, **16**(3), 1452–1475, DOI: 10.1038/s41596-020-00460-7.

9 S. Ghosh, K. Aggarwal, U. VT, T. Nguyen, J. Han and C. H. Ahn, A new microchannel capillary flow assay (MCFA) platform with lyophilized chemiluminescence reagents for a smartphone-based POCT detecting malaria, *Microsyst. Nanoeng.*, 2020, **6**, 5, DOI: 10.1038/s41378-019-0108-8.

10 C. S. Chuang, C. Z. Deng, Y. F. Fang, H. R. Jiang, P. W. Tseng, H. J. Sheen and Y. J. Fan, A Smartphone-based Diffusometric Immunoassay for Detecting C-Reactive Protein, *Sci. Rep.*, 2019, **9**(1), 17131, DOI: 10.1038/s41598-019-52285-4.

11 Y. Shen, J. Zhou, T. Liu, Y. Tao, R. Jiang, M. Liu, G. Xiao, J. Zhu, Z. K. Zhou, X. Wang, C. Jin and J. Wang, Plasmonic gold mushroom arrays with refractive index sensing figures of merit approaching the theoretical limit, *Nat. Commun.*, 2013, **4**, 2381, DOI: 10.1038/ncomms3381.

12 X. Ma, S. Song, S. Kim, M. S. Kwon, H. Lee, W. Park and S. J. Sim, Single gold-bridged nanoprobes for identification of single point DNA mutations, *Nat. Commun.*, 2019, **10**(1), 836, DOI: 10.1038/s41467-019-08769-y.

13 B. Karki, A. Pal, G. Dhiman and M. Z. Ahmed, Ultra-sensitive early detection of colorectal cancer using surface plasmon resonance sensor: theoretical analysis, *Mikrochim. Acta*, 2025, **192**(2), 126, DOI: 10.1007/s00604-025-06983-8.

14 H. Wang, S. Duan, M. Wang, *et al.*, Silk cocoon membrane-based immunosensing assay for red blood cell antigen typing, *Sens. Actuators, B*, 2020, **320**, 128376, DOI: 10.1016/j.snb.2020.128376.

15 B. Schuster, M. Junkin, S. S. Kashaf, I. Romero-Calvo, K. Kirby, J. Matthews, C. R. Weber, A. Rzhetsky, K. P. White and S. Tay, Automated microfluidic platform for dynamic and combinatorial drug screening of tumor organoids, *Nat. Commun.*, 2020, **11**(1), 5271, DOI: 10.1038/s41467-020-19058-4.

16 M. He, J. Novak, B. A. Julian and A. E. Herr, Membrane-assisted online renaturation for automated microfluidic lectin blotting, *J. Am. Chem. Soc.*, 2011, **133**(49), 19610–19613, DOI: 10.1021/ja207963f.

17 T. Hoshino, R. Nakao, H. Doi and T. Minamoto, Simultaneous absolute quantification and sequencing of fish environmental DNA in a mesocosm by quantitative sequencing technique, *Sci. Rep.*, 2021, **11**(1), 4372, DOI: 10.1038/s41598-021-83318-6.

18 Y. Li, J. D. Motschman, S. T. Kelly and B. B. Yellen, Injection Molded Microfluidics for Establishing High-Density Single Cell Arrays in an Open Hydrogel Format, *Anal. Chem.*, 2020, **92**(3), 2794–2801, DOI: 10.1021/acs.analchem.9b05099.

19 J. Zhou, Y. Zeng, X. Wang, *et al.*, The capture of antibodies by antibody-binding proteins for ABO blood typing using SPR

im-aging-based sensing technology, *Sens. Actuators, B*, 2019, **304**, 127391, DOI: 10.1016/j.snb.2019.127391.

20 X. Li, H. Feng, *et al.*, Capture of red blood cells onto optical sensor for rapid ABO blood group typing and erythrocyte counting, *Sens. Actuators, B*, 2018, **262**, 411–417, DOI: 10.1016/j.snb.2018.02.030.

21 A. Mujahid, S. Aigner, *et al.*, Micro-structured interdigital capacitors with synthetic antibody receptors for ABO blood-group typing, *Sens. Actuators, B*, 2017, **242**, 378–383, DOI: 10.1016/j.snb.2016.11.056.

22 P. Chinnawut, K. Chanwit, W. Thidarat, *et al.*, Polymethyl methacrylate (PMMA) point of care for ABO-Rh(D) blood typing, *Sens. Actuators, B*, 2018, **273**, 703–709, DOI: 10.1016/j.snb.2018.06.074.

23 P. Wang and R. Elena, Glucose sensing on reproducible and tunable plasmonic nanostructures formed on annealed coverslips coated with thin layers of gold and indium tin oxide, *Sens. Actuators, A*, 2021, **318**(1), 112510, DOI: 10.1016/j.sna.2020.112510.

24 P. Wang and R. E. Ionescu, Chemosensing on Miniaturized Plasmonic Substrates, *Micromachines*, 2021, **12**(3), 275, DOI: 10.3390/mi12030275.

25 Y. Chen, H. Fan, R. Li, H. Zhang, R. Zhou, G. L. Liu, C. Sun and L. Huang, Free Electron Density Gradients Enhanced Biosensor for Ultrasensitive and Accurate Affinity Assessment of the Immunotherapy Drugs, *Adv. Sci.*, 2024, **11**(46), e2404559, DOI: 10.1002/advs.202404559.

26 CLSI, *Evaluation of Stability of In Vitro Medical Laboratory Test Reagents*, CLSI Document EP25, Clinical and Laboratory Standards Institute, Karl De Vore, BA, 2ed edn, 2023.

27 S. Qiu, Y. Dong, X. Yu, Q. Ai, L. Yuan, L. Zhang and D. Zhang, Highly selective localized surface plasmon resonance sensor for selenium diagnosis in selenium-rich soybeans, *J. Hazard. Mater.*, 2024, **478**, 135632, DOI: 10.1016/j.jhazmat.2024.135632.

28 K. Jia, T. Toury and R. E. Ionescu, Fabrication of an atrazine acoustic immunosensor based on a drop-deposition procedure, *IEEE Trans. Ultrason. Ferroelectr. Freq. Control*, 2012, **59**(9), 2015–2021, DOI: 10.1109/TUFFC.2012.2421.

29 W. Tangkawsakul, T. Srikhirin, K. Shinbo, *et al.*, Application of long-range surface plasmon resonance for ABO blood typing, *Int. J. Anal. Chem.*, 2016, **2016**, 1432781, DOI: 10.1155/2016/1432781.

30 E. B. Aydın, M. Aydın and M. K. Sezgintürk, Highly selective and sensitive sandwich immunosensor platform modified with MUA-capped GNPs for detection of spike Receptor Binding Domain protein: A precious marker of COVID 19 infection, *Sens. Actuators, B*, 2021, **345**, 130355, DOI: 10.1016/j.snb.2021.130355.

31 J. Noiphung, K. Talalak, I. Hongwarittorrn, N. Pupinyo, P. Thirabowonkitphithan and W. Laiwattanapaisal, A novel paper-based assay for the simultaneous determination of Rh typing and forward and reverse ABO blood groups, *Biosens. Bioelectron.*, 2015, **67**, 485–489, DOI: 10.1016/j.bios.2014.09.011.

32 M. M. Langston, J. L. Procter, K. M. Cipolone and D. F. Stroncek, Evaluation of the gel system for ABO grouping and D typing, *Transfusion*, 1999, **39**(3), 300–305, DOI: 10.1046/j.1537-2995.1999.39399219288.x.